Impact of Surface Orientation on the Sensitivity of FinFETs to Process Variations—An Assessment Based on the Analytical Solution of the Schrödinger Equation

Yu-Sheng Wu, *Student Member, IEEE*, and Pin Su, *Member, IEEE*

***Abstract*—This paper investigates the impact of surface orientation on $V_{\rm th}$ sensitivity to process variations for Si and Ge fin-shaped field-effect transistors (FinFETs) using an analytical solution of the Schrödinger equation. Our theoretical model considers the parabolic potential well due to short-channel effects and, therefore, can be used to assess the quantum-confinement effect in short-channel FinFETs. Our study indicates that, for ultrascaled FinFETs, the importance of channel thickness ($t_{\rm ch}$) variations increases due to the quantum-confinement effect. The Si-(100) and Ge-(111) surfaces show lower $V_{\rm th}$ sensitivity to the $t_{\rm ch}$ variation as compared with other orientations. On the contrary, the quantum-confinement effect reduces the $V_{\rm th}$ sensitivity to the $L_{\rm eff}$ variation, and Si-(111) and Ge-(100) surfaces show lower $V_{\rm th}$ sensitivity as compared with other orientations. Our study may provide insights for device design and circuit optimization using advanced FinFET technologies.**

***Index Terms*—Fin-shaped field-effect transistor (FinFET), quantum effects, surface orientation, variation.**

I. Introduction

As THE carrier mobility of a MOSFET depends on surface orientation [1]–[3], it has been proposed that with an optimized surface orientation, the circuit performance of a fin-shaped field-effect transistor (FinFET) structure can be enhanced [3], [4]. However, with the scaling of device geometry, process variation has become a crucial issue. The immunity of a FinFET structure with various surface orientations to process variations is an important issue. In our previous work [5], we have investigated the threshold voltage ($V_{\rm th}$) sensitivity to process variations for lightly doped FinFETs using an analytical solution of Poisson's equation. As the channel thickness of the FinFETs scales down, nevertheless, the quantum-confinement effect may become significant. This 1-D confinement effect may result in a $V_{\rm th}$ shift and impact the $V_{\rm th}$ sensitivity to process variations. Moreover, the impact of quantum confinement may show surface-orientation dependence.

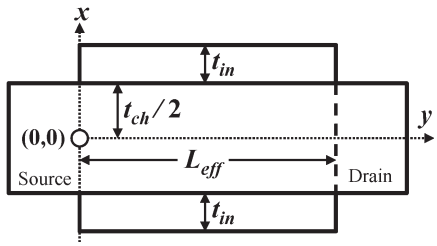

Fig. 1. Schematic of the FinFET structure investigated in this paper. $L_{\rm eff}$ is the channel length, $t_{\rm ch}$ is the channel thickness, and $t_{\rm in}$ is the gate-insulator thickness.

In this paper, we investigate the $V_{\rm th}$ sensitivity to process variations for Si- and Ge-channel FinFETs with various channel orientations using an analytical solution of the Schrödinger equation. For long-channel undoped devices, the quantum-confinement effect is often considered to be independent of the carrier-flow direction (i.e., channel-length direction), and the potential well in the Schrödinger equation is usually assumed to be flat [6]. For short-channel devices, however, the center of the potential well is altered by source/drain coupling due to short-channel effects, and flat-well approximation is no longer valid. Therefore, an accurate solution of the Schrödinger equation that considers the short-channel effect is crucial to the determination of $V_{\rm th}$ for ultrascaled FinFETs.

This paper is organized as follows. In Section II, we analytically derive the solution of the Schrödinger equation for the short-channel FinFETs under the subthreshold region, and the model results are verified with technology computer-aided design (TCAD) simulation. In Section III, we calculate the electron density and $V_{\rm th}$ using our theoretical model. Then, we investigate the $V_{\rm th}$ sensitivity to process variations for Si- and Ge-channel FinFETs with various surface orientations. Finally, the conclusion is drawn in Section IV.

II. Analytical Solution of the Schrödinger Equation and Verification With TCAD

Fig. 1 shows a schematic sketch of a FinFET structure. To consider the quantum-confinement effect along the fin-width (i.e., x) direction, the Schrödinger equation can be expressed as

$$-\frac{\hbar^2}{2m_x}\frac{d^2\Psi_j(x)}{dx^2}+E_C(x)\Psi_j(x)=E_j\Psi_j(x) \qquad (1)$$

Manuscript received July 15, 2010; revised September 15, 2010; accepted September 16, 2010. Date of publication October 18, 2010; date of current version November 19, 2010. This work was supported in part by the National Science Council (NSC) of Taiwan under Contract NSC 98-2221-E-009-178 and in part by the Ministry of Education in Taiwan under the Aim for the Top University Program. The review of this paper was arranged by Editor H. S. Momose.

The authors are with the Department of Electronics Engineering and Institute of Electronics, National Chiao Tung University, Hsinchu 30013, Taiwan (e-mail: pinsu@faculty.nctu.edu.tw).

Color versions of one or more of the figures in this paper are available online at http://ieeexplore.ieee.org.

Digital Object Identifier 10.1109/TED.2010.2080682

TABLE I
QUANTIZATION EFFECTIVE MASS (m_x) AND THE DENSITY-OF-STATE EFFECTIVE MASS (m_d) FOR THE ELECTRONS IN Si AND Ge CHANNELS WITH VARIOUS SURFACE ORIENTATIONS [8]

Surface orientation	Si			Ge		
	m_x	m_d	degeneracy	m_x	m_d	degeneracy
(100)	0.916 0.191	0.191 0.418	2 4	0.120	0.299	4
(110)	0.316 0.191	0.325 0.418	4 2	0.223 0.082	0.219 0.361	2 2
(111)	0.260	0.359	6	1.590 0.092	0.082 0.342	1 3

where E_j is the jth eigen-energy, $\Psi_j(x)$ is the corresponding wave function, $\hbar$ is the reduced Planck constant, and m_x is the carrier-quantization effective mass. For electrons in the Si and Ge channels, m_x for various surface orientations are listed in Table I. If the conduction band edge $E_C(x)$ is treated as a flat well with a potential energy β, the solution of (1) is $\Psi_j(x) = (2/t_{\rm ch})^{1/2}\sin[(j+1)\pi(x+t_{\rm ch}/2)/t_{\rm ch}]$ and $E_j = \beta + (j+1)^2\pi^2\hbar^2/(2m_x t_{\rm ch}^2)$ [6]. However, to account for the source/drain coupling due to short-channel effects, the conduction band edge $E_C(x)$ in (1) should be treated as a parabolic well with potential energy $E_C(x) = \alpha x^2 + \beta$ [7]. α and β are length-dependent coefficients and can be obtained from the channel potential solution of Poisson's equation under the subthreshold region.

In our previous work [5], we have derived the 3-D channel potential solution $\phi(x,y,z)$ for multigate MOSFETs in the subthreshold region. For the FinFET structure in this study, the potential solution can still be applied after neglecting the top-gate potential coupling along the fin-height direction. In other words, the channel potential solution for the FinFET structure in Fig. 1 can be expressed as $\phi(x,y) = \phi_1(x) + \phi_2(x,y)$, as given in (2a)–(2f), shown at the bottom of the page, where $W_{\rm eff} = t_{\rm ch} + 2(\varepsilon_{\rm ch}/\varepsilon_{\rm in})t_{\rm in}$ with $\varepsilon_{\rm ch}$ and $\varepsilon_{\rm in}$ being the dielectric constants of the channel and the gate insulator, respectively. $t_{\rm in}$ is the thickness of the gate insulator. N_a is the channel doping, V_{GS} is the voltage bias of the gate terminal, $V_{\rm fb}$ is the flat-band voltage, V_{DS} is the voltage bias of the drain terminal, and $\phi_{\rm ms}$ is the built-in potential of the source/drain to the channel.

After further reducing ϕ_2 to a parabolic form, E_C can be expressed as $E_C(x) = \alpha x^2 + \beta$ with

$$\alpha = (-q)\left(\sum_{i=1}^{\infty}\left\{c_i\sinh\left(\frac{i\pi}{W_{\rm eff}}y\right) + c_i'\sinh\left[\frac{i\pi}{W_{\rm eff}}(L_{\rm eff}-y)\right]\right\} \times\left[-\frac{1}{2}\left(\frac{i\pi}{W_{\rm eff}}\right)^2\right]\sin\left(\frac{i\pi}{2}\right)\right) \tag{3a}$$

$$\beta = (-q)\left(b+\sum_{i=1}^{\infty}\left\{c_i\sinh\left(\frac{i\pi}{W_{\rm eff}}y\right) + c_i'\sinh\left[\frac{i\pi}{W_{\rm eff}}(L_{\rm eff}-y)\right]\right\} \times\sin\left(\frac{i\pi}{2}\right) - \left[\frac{1}{2}\frac{E_g}{q} + \frac{1}{2}\frac{kT}{q}\ln\left(\frac{N_{\rm c}}{N_{\rm v}}\right)\right]\right) \tag{3b}$$

where kT/q is the thermal voltage, E_g is the bandgap of the channel material, and $N_{\rm c}$ and $N_{\rm v}$ are the effective density of

$$\phi_1(x) = -\frac{qN_a}{2\varepsilon_{\rm ch}}\left(x+\frac{1}{2}t_{\rm ch}\right)^2 + a\left(x+\frac{1}{2}t_{\rm ch}\right)+b \tag{2a}$$

$$a = \frac{(qN_a/2\varepsilon_{\rm ch})\left\{t_{\rm ch}^2 + 2\left(\varepsilon_{\rm ch}/\varepsilon_{\rm in}\right)\left[t_{\rm ch}^2 + 2\left(\varepsilon_{\rm ch}/\varepsilon_{\rm in}\right)t_{\rm in}t_{\rm ch}\right]\right\}}{W_{\rm eff}} \tag{2b}$$

$$b = (V_{\rm GS} - V_{\rm fb}) + \frac{\varepsilon_{\rm ch}}{\varepsilon_{\rm in}}t_{\rm in}a \tag{2c}$$

$$\phi_2(x,y) = \sum_{i=1}^{\infty}\left\{c_i\sinh\left(\frac{i\pi}{W_{\rm eff}}y\right) + c_i'\sinh\left[\frac{i\pi}{W_{\rm eff}}(L_{\rm eff}-y)\right]\right\}\sin\left[\frac{i\pi}{W_{\rm eff}}\left(x+\frac{1}{2}t_{\rm ch}+\frac{\varepsilon_{\rm ch}}{\varepsilon_{\rm in}}t_{\rm in}\right)\right] \tag{2d}$$

$$c_i = \frac{1}{\sinh\left[i\pi\left(L_{\rm eff}/W_{\rm eff}\right)\right]}\left\{2(-\phi_{\rm ms}+V_{\rm DS}-b)\frac{1-(-1)^i}{i\pi} + 2a\left[\frac{t_{\rm in}}{i\pi} + \frac{(W_{\rm eff}-t_{\rm in})(-1)^i}{i\pi}\right] + \frac{qN_a}{\varepsilon_{\rm ch}}\left[\frac{t_{\rm in}^2}{i\pi} - \frac{(W_{\rm eff}-t_{\rm in})^2(-1)^i}{i\pi} + 2W_{\rm eff}^2\frac{(-1)^i-1}{(i\pi)^3}\right]\right\} \tag{2e}$$

$$c_i' = \frac{1}{\sinh\left[i\pi\left(L_{\rm eff}/W_{\rm eff}\right)\right]}\left\{2(-\phi_{\rm ms}-b)\frac{1-(-1)^i}{i\pi} + 2a\left[\frac{t_{\rm in}}{i\pi} + \frac{(W_{\rm eff}-t_{\rm in})(-1)^i}{i\pi}\right] + \frac{qN_a}{\varepsilon_{\rm ch}}\left[\frac{t_{\rm in}^2}{i\pi} - \frac{(W_{\rm eff}-t_{\rm in})^2(-1)^i}{i\pi} + 2W_{\rm eff}^2\frac{(-1)^i-1}{(i\pi)^3}\right]\right\} \tag{2f}$$

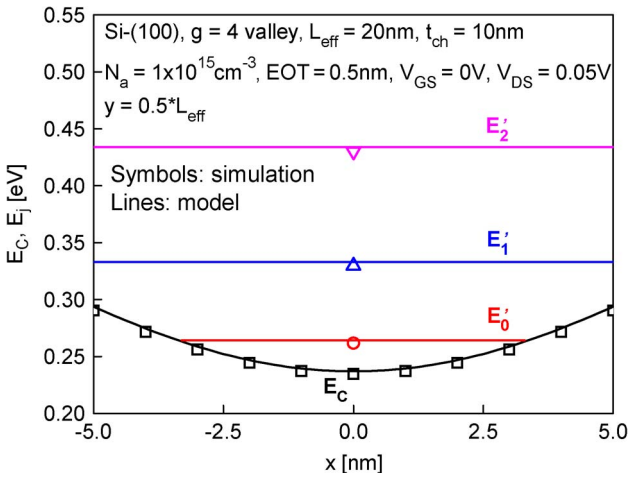

Fig. 2. Conduction-band edge and quantized eigen-energies of a short-channel lightly doped FinFET.

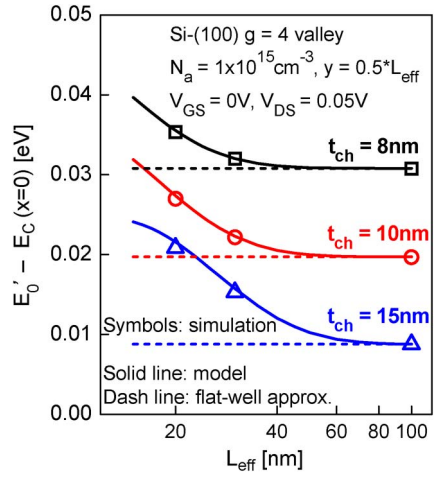

Fig. 3. Channel-length dependence of E_0' for lightly doped FinFETs with various $t_{\rm ch}$ showing the accuracy of our model.

states for conduction and valence bands, respectively. Using the parabolic-well approximation, the solution of (1) can be expressed as [9]

$$\Psi_j(x) = \sum_{n=0}^{\infty} d_n x^n \tag{4a}$$

with the coefficient d_n being determined by the following recurrence relationship:

$$d_2 = -\frac{m_x(E_j-\beta)}{\hbar^2}d_0 \qquad d_3 = -\frac{m_x(E_j-\beta)}{3\hbar^2}d_1$$
$$d_{n+2} = -\frac{2m_x(E_j-\beta)/\hbar^2}{(n+1)(n+2)} \times d_n + \frac{2m_x\alpha/\hbar^2}{(n+1)(n+2)}d_{n-2}, \qquad n \geq 2. \tag{4b}$$

It should be noted that as $\alpha = 0$ (i.e., E_C is spatially constant), $\Psi_j(x)$ will return to the form of sinusoidal functions, which is the solution for the flat-well approximation [6]. The jth eigen-energy E_j can be determined by the boundary condition $\Psi_j(x = t_{\rm ch}/2) = 0$. Thus, the eigen-energy and the eigenfunction of the short-channel FinFET under the subthreshold region can be derived.

To validate the accuracy of our model, we compare the calculation results with the TCAD simulation that numerically solves the self-consistent solution of the 2-D Poisson's and 1-D Schrödinger equations [10]. The Schrödinger equation is solved along the fin-width x-direction to consider the quantum-confinement effect. The effective masses used for various surface orientations in the TCAD simulations are listed in Table I. We assume that the barrier height across the gate insulator/channel is infinite, and the wave functions vanish at the interface. In this study, we focus on FinFETs with lightly doped channel $N_a = 10^{15}$ cm^{-3}. The equivalent oxide thickness is 0.5 nm to sustain the electrostatic integrity, and a midgap-gate work function (4.5 eV) is used. Fig. 2 shows that for a short-channel lightly doped FinFET, the conduction band edge E_C is bent from a flat well to a parabolic-like well due to the source/drain coupling. It can be seen that the eigen-

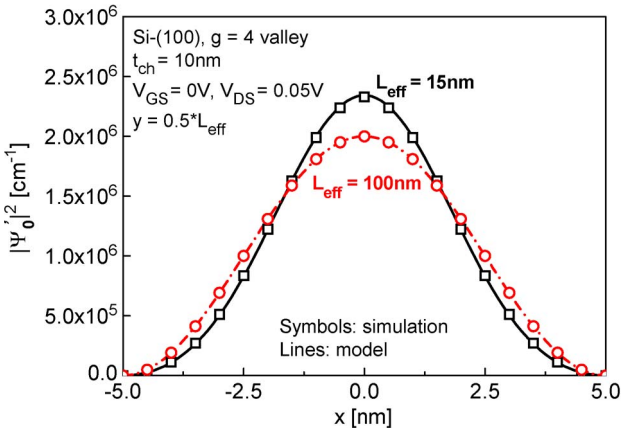

Fig. 4. Comparison of the square of Ψ_0' for long- and short-channel FinFETs.

energy calculated by our model considering the parabolic-well approximation agrees well with the TCAD simulation. Since E_C is not spatially constant along the x-direction for short-channel devices, we choose E_C at the channel center (i.e., $x = 0$) as the reference energy. Fig. 3 shows the channel-length ($L_{\rm eff}$) dependence of the energy difference of E_0' (ground-state energy in a fourfold valley) and the bottom of well $E_C(x = 0)$. In contrast to the constant $E_0' - E_C(x = 0)$ calculated from the flat-well approximation, both the TCAD simulation and our model show that $E_0' - E_C(x = 0)$ increases with decreasing $L_{\rm eff}$. In addition to eigen-energy, the bent potential well due to the short-channel effect also affects the shape of the wave function. Fig. 4 shows that $|\Psi_0'|^2$ for lightly doped FinFETs with shorter $L_{\rm eff}$ (i.e., $L_{\rm eff} = 15$ nm) is more centralized to the channel center. This is because the E_C barrier at the channel center $(x = 0)$ is lower than that near the insulator/channel interface $(x = 0.5t_{\rm ch})$, and, thus, the electron density becomes larger at $x = 0$.

III. Results and Discussion

To assess the impact of the quantum confinement on the threshold voltage $V_{\rm th}$, $V_{\rm th}$ is defined as the V_{GS} at which the average electron density of the cross section at $y = L_{\rm eff}/2$

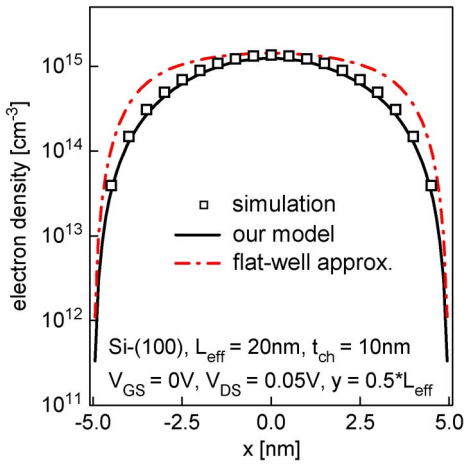

Fig. 5. Comparison of the electron density calculated from our model and the model using the flat-well approximation.

(the highest potential barrier for low V_{DS}) exceeds the critical concentration 1×10^{16} cm^{-3} [11]. The electron density is determined by the eigen-energy and eigenfunction as

$$n(x,y) = N_{C,\mathrm{QM}} \exp\left(-\frac{E_C - E_F}{kT}\right) \tag{5a}$$

$$N_{C,\mathrm{QM}} = \frac{kT}{\pi\hbar^2} \sum_{v,j} g_v m_d^v \left|\Psi_{v,j}(x,y)\right|^2 \exp\left(-\frac{E_{v,j} - E_C}{kT}\right) \tag{5b}$$

where g_v is the valley degeneracy, and m_d^v is the density-of-state effective mass of valley v. g_v and m_d^v for Si and Ge channels are listed in Table I. It can be seen from (5b) that the flat-well approximation may overestimate the electron density for short-channel devices because it underestimates the eigen-energy E_j (as shown in Fig. 3). Fig. 5 compares the electron density distribution calculated from the flat-well approximation and our model. The electron density predicted by our model agrees well with the TCAD simulation, whereas the flat-well approximation shows higher electron density in both sides of the channel.

For the FinFET structure, different surface orientations such as (100), (110), and (111) can be achieved by rotating the device layout in the wafer plane [3]. Fig. 6 shows that for Si FinFETs with a small t_{ch}, V_{th} and its sensitivity to channel thickness (t_{ch}) variations considering the quantum-confinement effect is larger than that predicted by the classical model (CL). Moreover, the V_{th} of the (111) and (110) surfaces increase more rapidly than that of the (100) surface with decreasing t_{ch}. This is because the quantum-confinement effect depends on the surface orientation, as indicated by the inset in Fig. 6. For a FinFET with a small t_{ch}, V_{th} is mainly determined by E_0. In addition, as m_x and, thus, the ground-state energy of twofold and fourfold valleys for (100) and (110) surfaces are different (see Table I), the overall lowest state occurs for the valley with larger m_x because (to the first order) the eigen-energy is inversely proportional to m_x. Therefore, the m_x of the twofold valley determines the E_0 for the (100) surface, and

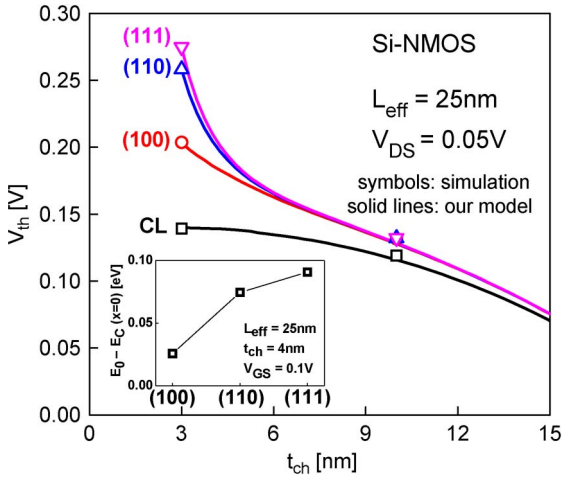

Fig. 6. Comparison of the t_{ch} dependence of V_{th} for Si FinFETs with various surface orientations and the CL. The V_{th} shift due to quantum confinement is mainly determined by E_0, as indicated by the inset.

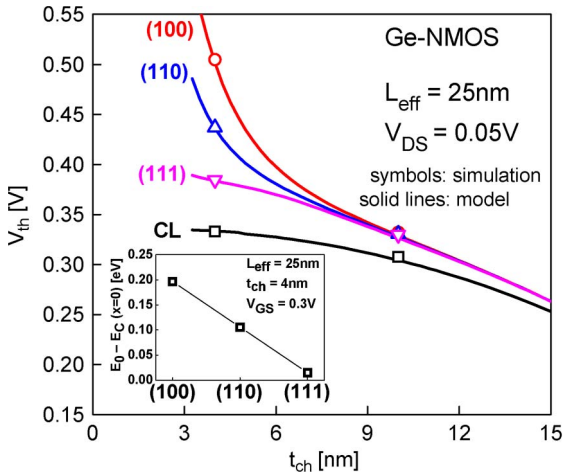

Fig. 7. Comparison of the t_{ch} dependence of V_{th} for Ge FinFETs with various surface orientations and the CL. (Inset) Comparison of E_0 for various surface orientations.

the m_x of the fourfold valley determines the E_0 for the (110) surface. Since the dominant m_x of various surface orientations for the Si channel is (111) $<$ (110) $<$ (100), the E_0 and, thus, V_{th} is (111) $>$ (110) $>$ (100), as shown in Fig. 6.

For a high-mobility channel such as Ge FinFETs, V_{th} dispersion due to quantum confinement becomes more significant. Fig. 7 shows that the V_{th} of the (100) surface increases more rapidly than the (110) and (111) surfaces with reducing t_{ch}. This is because the quantum-confinement effect of the (100) surface is larger than that of the (110) and (111) surfaces, as indicated by the inset in Fig. 7. Since the dominant m_x of the various surface orientations for the Ge channel is (111) $>$ (110) $>$ (100), the E_0 and V_{th} is (100) $>$ (110) $>$ (111).

Besides V_{th} sensitivity to t_{ch} variation, the quantum-confinement effect also affects V_{th} sensitivity to L_{eff} variation. Fig. 8 shows that for Ge FinFETs, the degree of V_{th} rolloff predicted by our quantum-confinement model is (100) $<$ (110) $<$ (111) $<$ CL, which is opposite to V_{th} sensitivity to t_{ch} variations (Fig. 7). In other words, while the quantum-confinement effect enhances V_{th} sensitivity to t_{ch} variation, it

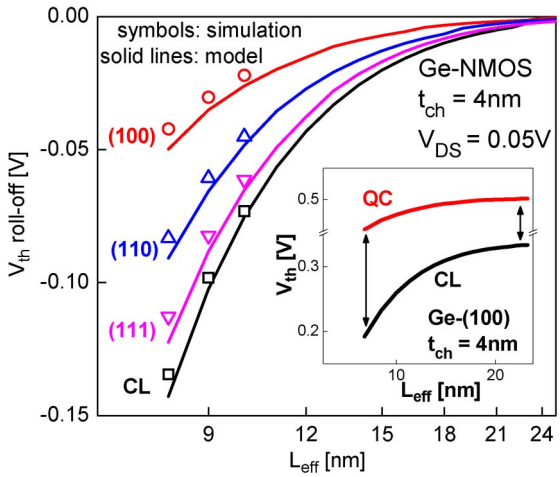

Fig. 8. Comparison of the $L_{\rm eff}$ dependence of $V_{\rm th}$ ($V_{\rm th}$ rolloff) for Ge FinFETs with various surface orientations and the CL. The $V_{\rm th}$ rolloff is defined as $V_{\rm th}$ ($L_{\rm eff}$) − $V_{\rm th}$ ($L_{\rm eff}$ = 100 nm). (Inset) Devices with smaller $L_{\rm eff}$ show larger $V_{\rm th}$ shift due to the quantum-confinement effect than the devices with larger $L_{\rm eff}$.

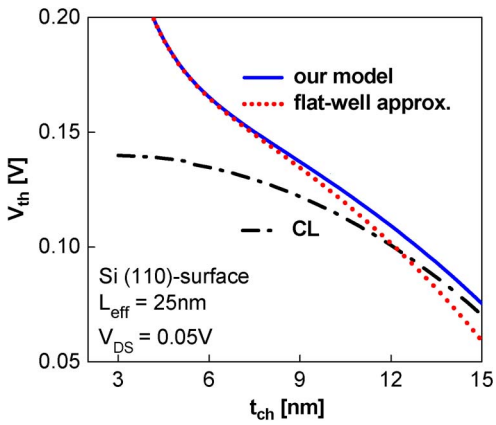

Fig. 9. Comparison of the $t_{\rm ch}$ dependence of $V_{\rm th}$ of the short-channel FinFETs calculated from the CL, our model, and the model using flat-well approximation.

reduces $V_{\rm th}$ sensitivity to $L_{\rm eff}$ variation. This can be explained as follows. The $V_{\rm th}$ shift due to the quantum-confinement effect can be expressed as $\Delta V_{\rm th}^{\rm QM} = S/(\ln 10\ kT/q)\Delta\Psi_s^{\rm QM}$, with S being the subthreshold swing and $\Delta\Psi_s^{\rm QM}$ being the equivalent surface potential shift [12]. The S for a short-channel device is larger than that for a long-channel device because of the enhanced drain coupling with decreasing $L_{\rm eff}$. Therefore, for devices with a given surface orientation, the $\Delta V_{\rm th}^{\rm QM}$ (which increases $V_{\rm th}$) of the short-channel device is larger than that of the long-channel one, as indicated by the inset in Fig. 8. The discrepancy in $\Delta V_{\rm th}^{\rm QM}$ between short- and long-channel devices reduces the $V_{\rm th}$ rolloff, and the $V_{\rm th}$ rolloff considering the quantum-confinement effect becomes smaller than the CL. In addition, as $\Delta\Psi_s^{\rm QM}$ is determined by E_0, a larger E_0 (and, thus, $\Delta\Psi_s^{\rm QM}$) results in a larger $\Delta V_{\rm th}^{\rm QM}$ and, hence, smaller $V_{\rm th}$ rolloff. This explains why the degree of $V_{\rm th}$ rolloff is (100) < (110) < (111) for Ge FinFETs.

In addition to the eigen-energies (Fig. 3) and the electron density (Fig. 5), $V_{\rm th}$ calculated by our model is physically more accurate than that calculated by the flat-well approximation. Fig. 9 shows that $V_{\rm th}$ calculated using our model and the flat-well approximation are fairly close for devices with a small $t_{\rm ch}$. However, the discrepancy between the two models increases with $t_{\rm ch}$ because the impact of short-channel effects becomes more significant for devices with a larger $t_{\rm ch}$. Compared with the flat-well approximation, $V_{\rm th}$ calculated by our model is more physical because it returns to the classical one for devices with larger $t_{\rm ch}$, in which the quantum-confinement effect is negligible.

IV. Conclusion

We have investigated the impact of surface orientation on $V_{\rm th}$ sensitivity to process variations for Si and Ge FinFETs using an analytical solution of the Schrödinger equation. Our theoretical model considers the parabolic potential well due to short-channel effects and, therefore, can be used to assess the quantum-confinement effect in short-channel FinFETs. Our study indicates that, for ultrascaled FinFETs, the importance of channel thickness variations increases due to the quantum-confinement effect. The Si-(100) and Ge-(111) surfaces show lower $V_{\rm th}$ sensitivity to $t_{\rm ch}$ variation as compared with other orientations. On the contrary, the quantum-confinement effect reduces $V_{\rm th}$ sensitivity to $L_{\rm eff}$ variation, and Si-(111) and Ge-(100) surfaces show lower $V_{\rm th}$ sensitivity as compared with other orientations. Our study may provide insights for device design and circuit optimization using advanced FinFET technologies.

References

[1] M. Yang, E. P. Gusev, M. Ieong, O. Gluschenkov, D. C. Boyd, K. K. Chan, P. M. Kozlowski, C. P. D'Emic, R. M. Sicina, P. C. Jamison, and A. I. Chou, "Performance dependence of CMOS on silicon substrate orientation for ultrathin oxynitride and HfO_2 gate dielectrics," *IEEE Electron Device Lett.*, vol. 24, no. 5, pp. 339–341, May 2003.

[2] E. Landgraf, W. Rösner, M. Städele, L. Dreeskornfeld, J. Hartwich, F. Hofmann, J. Kretz, T. Lutz, R. J. Luyken, T. Schulz, M. Specht, and L. Risch, "Influence of crystal orientation and body doping on trigate transistor performance," *Solid State Electron.*, vol. 50, no. 1, pp. 38–43, Jan. 2006.

[3] L. Chang, M. Ieong, and M. Yang, "CMOS circuit performance enhancement by surface orientation optimization," *IEEE Trans. Electron Devices*, vol. 51, no. 10, pp. 1621–1627, Oct. 2004.

[4] S. Gangwal, S. Mukhopadhyay, and K. Roy, "Optimization of surface orientation for high-performance, low-power and robust FinFET SRAM," in *Proc. IEEE CICC*, 2006, pp. 433–436.

[5] Y.-S. Wu and P. Su, "Sensitivity of multigate MOSFETs to process variations—An assessment based on analytical solutions of 3-D Poisson's equation," *IEEE Trans. Nanotechnol.*, vol. 7, no. 3, pp. 299–304, May 2008.

[6] H. Ananthan and K. Roy, "A compact physical model for yield under gate length and body thickness variations in nanoscale double-gate CMOS," *IEEE Trans. Electron Devices*, vol. 53, no. 9, pp. 2151–2159, Sep. 2006.

[7] Y.-S. Wu and P. Su, "Quantum confinement effect in short-channel gate-all-around MOSFETs and its impact on the sensitivity of threshold voltage to process variations," in *Proc. IEEE Int. SOI Conf.*, 2009, pp. 1–2.

[8] F. Stern and W. E. Howard, "Properties of semiconductor surface inversion layers in the electric quantum limit," *Phys. Rev.*, vol. 163, no. 3, pp. 816–835, Nov. 1967.

[9] D. G. Zill and M. R. Cullen, *Differential Equations With Boundary Value Problems,* 5th ed. Pacific Grove, CA: Brooks/Cole, 2001.

[10] ATLAS User's Manual, SILVACO, Santa Clara, CA, 2008.

[11] C.-T. Lee and K. K. Young, "Submicrometer near-intrinsic thin-film SOI complementary MOSFETs," *IEEE Trans. Electron Devices*, vol. 36, no. 11, pp. 2537–2547, Nov. 1989.

[12] Y. Taur and T. H. Ning, *Fundamentals of Modern VLSI Devices*. Cambridge, U.K.: Cambridge Univ. Press, 1998.

Yu-Sheng Wu (S'09) was born in Tainan, Taiwan, in 1982. He received the B.S. and M.S. degrees in electronics engineering in 2004 and 2006, respectively, from the National Chiao Tung University, Hsinchu, Taiwan, where he is currently working toward the Ph.D. degree in the Institute of Electronics.

His current research interests include design and modeling of advanced CMOS devices.

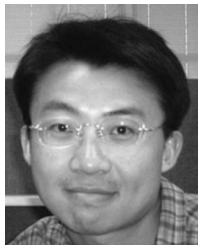

Pin Su (S'98–M'02) received the B.S. and M.S. degrees in electronics engineering from the National Chiao Tung University, Hsinchu, Taiwan, and the Ph.D. degree from the University of California, Berkeley.

From 1997 to 2003, he conducted his doctoral and postdoctoral research in silicon-on-insulator (SOI) devices in Berkeley. He was also one of the major contributors to the unified BSIMSOI model, which is the first industrial standard SOI MOSFET model for circuit design. Since August 2003, he has been with the Department of Electronics Engineering, National Chiao Tung University, where he is currently an Associate Professor. He has authored or coauthored over 100 research papers in refereed journals and international conference proceedings. His research interests include silicon-based nanoelectronics, modeling and design for advanced CMOS devices, and device and circuit interactions in nano-CMOS.